AN AUTOMATED METHOD TO CORRECT HELIOSTAT TRACKING ERRORS

Siri Sahib S. Khalsa[1], Clifford K. Ho[2], and Charles E. Andraka[2]

[1] Sandia Staffing Alliance, Under Contract to Sandia National Laboratories, P.O. Box 5800, Albuquerque, NM 87185-1127

[2] Sandia National Laboratories, Concentrating Solar Technologies Dept., P.O. Box 5800, Albuquerque, NM 87185-1127

Abstract

Accurate heliostat tracking is critical for the overall performance and efficiency of a central receiver concentrating solar power plant. Subtle errors in the fabrication and installation of heliostats can cause tracking errors that change throughout the day and year due to their non-linear dependence on the intended pointing vectors. The impact of these errors is exacerbated when a heliostat is located far from its target and can cause the reflected beam to miss the target, resulting in inefficiencies in the power plant's performance. It is typically not feasible to repair these fabrication and installation errors after heliostats are installed. Implementing a fixed pointing offset is usually ineffective due to the dependence of the errors on the time of day, day of the year, and target location. This paper describes an automated open-loop eight-dimensional tracking error characterization and correction method that is suitable for large heliostat fields, as it does not require any physical modification to the heliostats and may allow for a more rapid data collection relative to methods that use on-axis tracking. Tests are performed on a heliostat at the National Solar Thermal Test Facility at Sandia National Laboratories in Albuquerque, NM using this method, and analyses are performed to evaluate the relative contributions of the various error sources. Uncorrected heliostat pointing errors ranging from 4.0 – 8.3 mrad in azimuth and 4.7 – 7.2 mrad in elevation are reduced to rms errors of 0.4 mrad in azimuth and 0.1 mrad in elevation, in the presence of wind speeds as high as 20 mph.

Keywords: heliostat, tracking, error correction, error sources, alignment

1. Introduction

Heliostat tracking has been recognized for many years as a potential source of error that can impact the performance of central receiver systems. Baheti and Scott [1] identified several physical factors that contribute to tracking errors, which include pedestal tilt, elevation and azimuth reference biases, and deviations in the azimuth and elevation wheel sizes (linear errors that can also represent errors in gear ratios). They derived an algorithm to minimize the impacts of these errors by recording the differences in the desired and actual elevation and azimuthal angles while tracking the sun. The method uses a least-squares algorithm to yield six coefficients that are determined from these error measurements and describe physical error sources. As more measurements are made, the coefficients can be refined to further reduce the tracking error. In theory, these correction coefficients can be determined from a minimal set of measurements (e.g., over the course of a single day). Once determined, they can be applied to the tracking algorithm to improve the heliostat-tracking performance throughout the year (i.e., at different times and with different targets than those that were used for the error parameter estimation), presuming that the correction coefficients are indeed correlated to physical tracking errors. Edwards [3] proposed a similar method to reduce tracking errors for paraboloidal collectors using an optimization algorithm that minimizes the difference between a set of measured pointing directions and the corresponding set of actuator positions.

From 1981 to 1986, Mavis [5] performed studies to characterize the heliostat beam and tracking performance of the 10 MWe Solar One central receiver pilot plant. Factors that were identified as potentially contributing to errors in heliostat tracking included pedestal tilt, non-orthogonality between the elevation and azimuth axes, mirror canting inaccuracies, gravity loading and deformation, encoder resolution and bias error, and errors in the surveyed location of the heliostat. Tests showed that heliostats exhibited non-orthogonality errors and tilt errors, even though the heliostats were leveled during installation. Encoder bias error was also observed in plots of azimuthal error. To correct for these errors, a video-based beam characterization system

was used to determine the centroids of heliostat beams focused onto a target mounted on the tower. The X- and Y-offsets of the beam centroids relative to the desired aimpoints were determined at three different times during one day. These offsets were used in the heliostat controller to provide a "bias update" for the azimuthal and elevation encoder reference marks. Unlike the Baheti and Scott method, this correction method does not account for transient changes in the tracking error caused by different orientations of the heliostat during different times of the year.

Maish [6] described the development of a tracking controller using the formulation of Baheti and Scott to determine the six correction coefficients. The application for this controller was directed at solar arrays that tracked the sun (e.g., photovoltaic modules). Application to heliostats for central receivers was not described.

Stone and Jones [8] and Jones and Stone [10] discussed various errors sources and strategies to improve heliostat tracking for Solar Two, the successor to Solar One. Strategies included (1) using tracking accuracy data to change the azimuthal and elevation encoder reference marks (similar to the method used in [5]), (2) using tracking accuracy data to calculate an offset in the prescribed location of the heliostat used in the controller, and (3) implementing an error-correction model in the control system that eliminates time-variant tracking errors. The first two strategies were described as "band-aids" that serve to minimize the problem without actually solving it. The third strategy "solves" the problem, but the authors believed that it would be difficult to implement in the Solar Two heliostat control System. This third strategy is the same as the method proposed by Baheti and Scott, and it is the basis for the current work.

More recently, several studies have been published that describe a general sun-tracking formula for arbitrarily oriented heliostats and targets [12], integration of an on-axis general sun-tracking formula with an open-loop sun-tracking system [14], and development of tracking formulas and strategies for receiver-oriented spinning-elevation tracking of a toroidal heliostat [16]. In [14], three "misalignment angles" were determined from a general tracking formula to compensate for misalignment of the concentrator during installation. They performed a test to show that the determination and implementation of these misalignment angles in the general tracking formula improved the tracking of their on-axis solar collector.

In the current work, the derivation of Baheti and Scott is extended to a reflected beam (as opposed to on-axis tracking of the sun), and two additional error sources are considered to account for non-orthogonality between the elevation and azimuth drive-axes, and a boresight error introduced during facet canting. These extensions improve the method's suitability for large heliostat fields, as it now avoids any physical modification to the heliostats (as is typically required for on-axis tracking of the sun), and potentially reduces the time required to develop error models for each heliostat (relative to on-axis tracking of the sun). Tests are performed on heliostats at the National Solar Thermal Test Facility in Albuquerque, NM, using this new algorithm, and analyses are performed to evaluate the relative contribution of the various error sources.

2. Error Model

The magnitudes of the fabrication and installation errors on a heliostat are estimated by fitting observed errors in the reflected beam centroid location to an expression that characterizes the behavior of the physical error sources, as a function of the intended heliostat pointing angles. If all the important error sources are correctly characterized, then this method could be expected to accurately extrapolate tracking error corrections to any time of day, day of year, and desired beam target. Hence, this method most likely requires fewer observations than a method that fits observations to an arbitrary high-order polynomial, which relies on interpolation and may not be appropriate for extrapolation.

2.1. New Error Sources: Drive-Axis Non-Orthogonality and Boresight Error

The two error parameters appended to the original formulation of [1] describe drive-axis non-orthogonality and boresight error. Drive-axis non-orthogonality refers to a non-square attachment between the elevation and azimuth drive-axes, which results in an azimuthal pointing error that increases with the elevation angle. A boresight error is introduced when the heliostat facets are canted to focus along an optical axis that

deviates from the pointing vector defined by the drive-axes. A boresight error also results in an azimuthal pointing error that increases with the elevation angle. A boresight error may not be captured by error estimation methods that use on-axis tracking, and its consideration is important to allow the beam reflected onto a target to be used for error estimation. If a boresight error were neglected while using a reflected beam for error parameter estimation, then the boresight error could significantly reduce the accuracy of the estimates for the other error sources.

2.1.1. Drive-Axis Non-Orthogonality Characterization

(a) illustrates a non-orthogonality error. The drive axes are designed such that the *nominal elevation drive-axis* (Y) is perpendicular to the *azimuthal drive-axis* (Z). However, a non-square attachment between the two drive axes results in the *true elevation drive-axis* (Y') being rotated by an angle ε_7 away from the expected Y-axis. The elevation drive-axis, which has a non-orthogonality angle ε_7, is rotated through an angle α. The starting pointing vector $\hat{p}_0$ is elevated to $\hat{p}'$, which is given a resultant azimuthal error $\Delta\theta$. This section derives the behavior of $\Delta\theta$ as a function of the elevation angle α.

Consider a pointing vector $\hat{p}_0$ that starts with zero-elevation. The Y'-axis is driven in an attempt to set the elevation angle to α. The actual resulting pointing vector $\hat{p}'$ has an azimuthal error $\Delta\theta$ caused by the non-orthogonality error ε_7. The vector $\hat{p}'$ is given by:

$$\hat{p}' = \mathbf{R}_X(\varepsilon_7)\mathbf{R}_Y(\alpha)\mathbf{R}_X(-\varepsilon_7)\hat{p}_0 \tag{1}$$

where $\mathbf{R}_X$ and $\mathbf{R}_Y$ are matrices corresponding to clockwise rotations about the X and Y axes, respectively, and clockwise is defined when viewing the origin from the positive axes. Eq. 1 yields the following expression for $\hat{p}'$:

$$\hat{p}' = \begin{pmatrix} \hat{p}'_X \\ \hat{p}'_Y \\ \hat{p}'_Z \end{pmatrix} = \begin{pmatrix} \cos\alpha \\ \sin\varepsilon_7 \sin\alpha \\ \cos\varepsilon_7 \sin\alpha \end{pmatrix} \approx \begin{pmatrix} \cos\alpha \\ \varepsilon_7 \sin\alpha \\ \sin\alpha \end{pmatrix} \tag{2}$$

Eq. 2 assumes ε_7 is small and makes the first-order approximations $\sin\varepsilon_7 \approx \varepsilon_7$ and $\cos\varepsilon_7 \approx 1$. Eq. 2 yields the following expression for the azmiuthal error $\Delta\theta$:

$$\tan\Delta\theta = \frac{\hat{p}'_Y}{\hat{p}'_X} \approx \varepsilon_7 \tan\alpha \tag{3}$$

This error can be included directly in the least-squares formulation of Baheti and Scott when $\Delta\theta$ is sufficiently small, such that $\tan\Delta\theta \approx \Delta\theta$, yielding:

$$\Delta\theta \approx \varepsilon_7 \tan\alpha \tag{4}$$

The discrepancy between $\Delta\theta$ values calculated from Eqs. 3 and 4 is small for the majority of elevation angles. When ε_7 = 1 mrad, this discrepancy is less than 1% for elevation angles less than 89.7°. When ε_7 = 10 mrad, this discrepancy is less than 1% for elevation angles less than 86.7°.

2.1.2. Boresight Error Characterization

In (b), the optical axis $\hat{p}_0$ is misaligned with the nominal X-axis due to a boresight error of $\varepsilon_{8,\theta}$ in azimuth and $\varepsilon_{8,\alpha}$ in elevation. The rotation of the elevation drive-axis elevates $\hat{p}_0$ to $\hat{p}'$ and results in an azimuthal error $\Delta\theta$. This section derives the behavior of $\Delta\theta$ as a function of the elevation angle α.

The true pointing vector that corresponds to a nominally zero-elevation and zero-azimuth is given by:

$$\hat{p}_0 = \begin{pmatrix} \hat{p}_{0,X} \\ \hat{p}_{0,Y} \\ \hat{p}_{0,Z} \end{pmatrix} = \begin{pmatrix} \cos\varepsilon_{8,\alpha}\cos\varepsilon_{8,\theta} \\ \cos\varepsilon_{8,\alpha}\sin\varepsilon_{8,\theta} \\ \sin\varepsilon_{8,\alpha} \end{pmatrix} \tag{5}$$

The elevation drive-axis is turned by an angle α, converting $\hat{p}_0$ into $\hat{p}'$, which is given by:

$$\hat{p}' = \mathbf{R}_Y(\alpha)\hat{p}_0 = \begin{pmatrix} \cos\alpha\cos\varepsilon_{8,\alpha}\cos\varepsilon_{8,\theta} - \sin\alpha\sin\varepsilon_{8,\alpha} \\ \cos\varepsilon_{8,\alpha}\sin\varepsilon_{8,\theta} \\ \sin\alpha\cos\varepsilon_{8,\alpha}\cos\varepsilon_{8,\theta} + \cos\alpha\sin\varepsilon_{8,\alpha} \end{pmatrix} \approx \begin{pmatrix} \cos\alpha \\ \varepsilon_{8,\theta} \\ \sin\alpha + \varepsilon_{8,\alpha}\cos\alpha \end{pmatrix} \tag{6}$$

Eq. 6 assumes $\varepsilon_{8,\theta}$ and $\varepsilon_{8,\alpha}$ are small and makes first-order approximations similar to those used in Eq. 2. Eq. 6 yields the following expression for the azmiuthal error $\Delta\theta$:

$$\tan\Delta\theta = \frac{\hat{p}'_Y}{\hat{p}'_X} \approx \frac{\varepsilon_{8,\theta}}{\cos\alpha} \tag{7}$$

The same approximation used in Eq. 4 ($\Delta\theta$ is sufficiently small such that $\tan\Delta\theta \approx \Delta\theta$) can be used in Eq. 7, yielding:

$$\Delta\theta \approx \frac{\varepsilon_{8,\theta}}{\cos\alpha} \tag{8}$$

A boresight error also introduces an error in elevation, which is constant and equal to $\varepsilon_{8,\alpha}$ within the small angle approximation. Therefore, the elevation error introduced by a boresight error will behave like an elevation reference offset and does not need to be treated separately from the elevation reference offset already considered by the Baheti and Scott formulation.

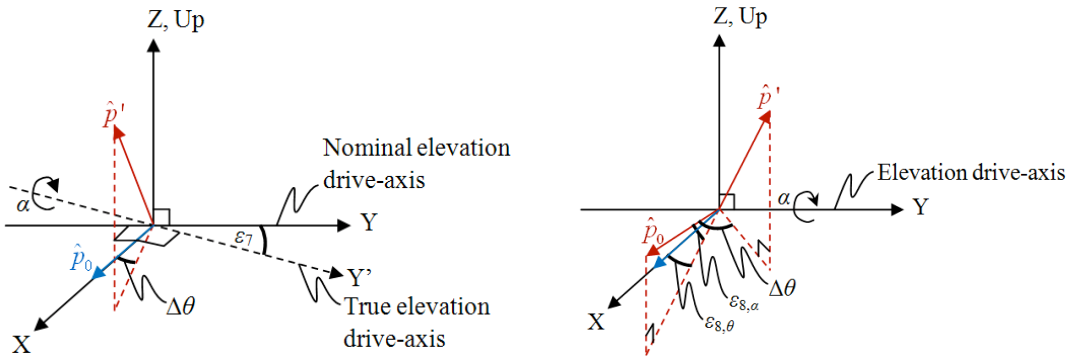

Fig. 1. Illustrations used to characterize the behavior of (a) drive-axis non-orthogonality error, and (b) boresight error.

2.2. Overall Error Model

Suppose a heliostat is instructed to point at an azimuthal angle θ and an elevation angle α. Assuming that the eight heliostat installation and fabrication errors are small (such that $\sin\varepsilon \approx \varepsilon$ and $\cos\varepsilon \approx 1$), the resultant pointing errors $\Delta\theta$ in azimuth and $\Delta\alpha$ in elevation are given by:

$$\begin{pmatrix} \Delta\theta \\ \Delta\alpha \end{pmatrix} = \mathbf{H}\boldsymbol{\varepsilon} \tag{9}$$

$$\text{where } \mathbf{H} \equiv \begin{pmatrix} \sin\theta\tan\alpha & \cos\theta\tan\alpha & 1 & 0 & \theta & 0 & \tan\alpha & \dfrac{1}{\cos\alpha} \\ \cos\theta & -\sin\theta & 0 & 1 & 0 & \alpha & 0 & 0 \end{pmatrix} \text{ and } \boldsymbol{\varepsilon} \equiv \begin{pmatrix} \varepsilon_1 \\ \varepsilon_2 \\ \varepsilon_3 \\ \varepsilon_4 \\ \varepsilon_5 \\ \varepsilon_6 \\ \varepsilon_7 \\ \varepsilon_8 \end{pmatrix}$$

The error parameters ε_1 and ε_2 represent pedestal tilt, ε_3 and ε_4 represent reference biases, ε_5 and ε_6 represent linear errors in azimuth and elevation (such as errors in the drive-wheel radii or gear ratios), ε_7 represents drive-axis non-orthogonality, and ε_8 represents boresight error. The behavior of parameters ε_1 through ε_6 is derived in [1].

3. Error Estimation and Correction

3.1. Error Estimation

The error parameter vector $\boldsymbol{\varepsilon}$ can be estimated by fitting observed errors in the reflected beam centroid to the error model described by Eq. 1 using least squares regression or another parameter estimation technique. The error estimation algorithm will, for each heliostat, (1) instruct the heliostat to reflect a beam onto a target, (2) take a photograph of the illuminated target to calculate the actual location of the reflected beam centroid, (3) calculate the observed heliostat pointing errors using the locations of the heliostat, sun, intended target, and reflected beam centroid, (4) repeat steps 1-3 for other targets, and (5) fit the observed pointing errors to Eq. 9 when a sufficient number of observations have been made. The error parameter vector $\boldsymbol{\varepsilon}$ can be estimated from a list of observations of $\Delta\theta$ and $\Delta\alpha$ for various heliostat pointing angles, using the least-squares algorithm in Eq. 10 or other parameter estimation method [1],[17]:

$$\boldsymbol{\varepsilon} = \left[\sum_{k=1}^{L} \mathbf{H}^{\mathrm{T}}(k)\mathbf{H}(k)\right]^{-1}\left[\sum_{k=1}^{L} \mathbf{H}^{\mathrm{T}}(k)\mathbf{q}(k)\right] \tag{10}$$

where L is the total number of observations of $\Delta\theta$ and $\Delta\alpha$. This process can be repeated at different times of the day to mitigate the impact of random errors, such as drive backlash, wind deflections, etc. The accuracy of the error estimation is favored when the observations span a wide range of heliostat pointing angles. Error correction methods that use on-axis tracking can make only one effective observation at a given time of the day. However, when the reflected beam is used, the heliostat can reflect the sun onto targets at different locations in immediate succession, thereby sampling a wider range of pointing angles at a time and accelerating the error estimation process.

3.2 Error Correction

After the error parameter vector ε has been estimated for a particular heliostat, its pointing errors can be predicted for any set of intended pointing angles, which allows for the error correction algorithm to compensate for their effects. Suppose the heliostat must point with an azimuthal angle θ and an elevation angle α in order to focus a beam onto the receiver. If the heliostat were instructed to point with these angles θ and α, then the tracking errors may cause the beam to miss the intended target. Instead, the error correction algorithm instructs the heliostat to point with some other angles, θ' and α', such that Eq. 11 is satisfied with θ' and α' used in $\mathbf{H}$.

$$\begin{pmatrix} \theta \\ \alpha \end{pmatrix} = \begin{pmatrix} \theta' \\ \alpha' \end{pmatrix} + \mathbf{H}\boldsymbol{\varepsilon} \tag{11}$$

Eq. 11 can be solved numerically by iterating in only one dimension, because α' can be expressed in terms of θ' and other known parameters. The numerical algorithm searches for the angle θ' that satisfies Eq. 12, which is yielded by rearranging Eq. 9. The required value of α' is then calculated directly from the resulting θ'.

$$\theta = \theta' + \varepsilon_1 \sin\theta' \tan\alpha' + \varepsilon_2 \cos\theta' \tan\alpha' + \varepsilon_3 + \varepsilon_5 \theta' + \varepsilon_7 \tan\alpha' + \frac{\varepsilon_8}{\cos\alpha'} \tag{12}$$

$$\text{where } \alpha' = \frac{\alpha - \varepsilon_1 \cos\theta' + \varepsilon_2 \sin\theta' - \varepsilon_4}{1 + \varepsilon_6}$$

If the heliostat is instructed to point at these calculated angles θ' and α' then, if the algorithm was successful, the true resultant heliostat pointing angles will be the desired θ and α and the beam will focus onto the intended target.

4. On-Sun Test

4.1. Objective and Test Overview

An on-sun test was performed using a heliostat at the National Solar Thermal Test Facility (NSTTF) at Sandia National Laboratories in Albuquerque, NM, with the objective of evaluating the effectiveness of the error correction method described in Section 3.

The heliostat "12E13" used for the test was located 121.9m East and 145.7m North of the center of the tower's front face. The heliostat's pedestal was tilted by approximately 0.5° to the East in order to exacerbate its tracking errors. The heliostat was then used to focus the sun onto the North face of the tower (Fig. 2), and its tracking errors were measured using photos taken of the beam on the tower on June 16 and 17, 2011. The method described in Section 3 was used in an attempt to compensate for these errors, and the resulting improved tracking errors were measured for several hours on July 15, 2011.

Fig. 2. Photograph of heliostat 12E13 at the NSTTF in Albuquerque, NM, focusing the sun onto the tower's North face.

4.2. Error Measurement Method and Apparatus

The position of the beam on the North face of the tower was used to calculate the heliostat pointing errors. The beam position was calculated using photographs taken from the control room of the NSTTF, approx. 360m North of the tower (Fig. 4). Photographs of the beam were taken using a tripod-mounted Basler A102f camera, equipped with a Nikon AF VR-NIKKOR 80-400mm zoom lens, and a Quantaray 2x AF tele-converter (used to double the camera's focal length). Images were captured on a desktop computer using an image acquisition tool written in MATLAB. The image acquisition tool was used to remove background noise from the beam images and calculate the position of the beam centroid. Two reference holes on the North face of the tower with known locations were captured in the same frame as the beam images. These reference holes were used for rotational reference (to determine the East and Up vectors on the images) and spatial reference (to calculate the vertical and horizontal pixel-to-meter conversion factors).

Fig. 4. Photograph of apparatus used to measure beam position on the tower.

4.3. Tracking Error Observations before Corrections and Error Parameter Estimation

Tracking errors of the heliostat were observed from 12:30 p.m. – 4:40 p.m. on June 16, 2011 and from 9:30 a.m. – 3:55 p.m. on June 17, 2011. Aim points on the North face of the tower were located 2m West of the tower centerline and were varied from 21.5m – 24.9m above the ground in order to increase the span of data collected at a given time of day. Both days featured wind speeds from 10 mph to over 25 mph from the Southwest, scattered clouds, and a significant amount of smoke produced by the Wallow fire in Arizona and western New Mexico. Images were captured at an interval of ~15-30 minutes and at a frame rate of 2 frames per second for 30 seconds, in order to resolve tracking error fluctuations due to heliostat shaking in the presence of wind. The heliostat pointing errors in azimuth and elevation were calculated from the images and used in Eq. 10 to estimate the error parameter vector (Table 1). The value $\varepsilon_2 = 8.84\text{x}10^{-3}$ rad = 0.506°, calculated using the observed pointing errors in the images, is consistent with the deliberately induced ~0.5° tilt of the heliostat to the East.

Table 1. Elements of error parameter vector calculated from observations on June 16-17, 2011.

Pedestal Tilt to North or South, ε_1	**Pedestal Tilt to East or West, ε_2**	**Azimuth Reference Bias, ε_3**	**Elevation Reference Bias, ε_4**	**Azimuth Linear Error, ε_5**	**Elevation Linear Error, ε_6**	**Drive-Axis Non-Orthogonality, ε_7**	**Boresight Error, ε_8**
$9.06\text{x}10^{-4}$ rad	$8.84\text{x}10^{-3}$ rad	$-1.10\text{x}10^{-4}$ rad	$-1.40\text{x}10^{-3}$ rad	$-6.84\text{x}10^{-5}$	$1.23\text{x}10^{-3}$	$-3.47\text{x}10^{-3}$ rad	$3.87\text{x}10^{-3}$ rad

The goodness-of-fit of the error model was checked by comparing the observed heliostat pointing errors with the pointing errors predicted by Eq. 9 using this error parameter vector (Fig. 6). The agreement is good, which indicates that the error model correctly describes the observed error behavior. Note that the pointing errors vary significantly throughout the day, indicating that a fixed correction bias alone would be insufficient to rectify the errors. The observed fluctuations in heliostat pointing error for a given time of day in Fig. 6 occur over a 30-second interval and are most likely due to heliostat shaking in the presence of the 10-25 mph winds.

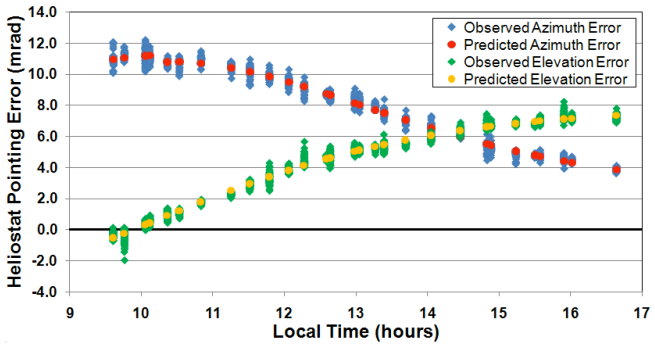

Fig. 6. Plot of heliostat pointing errors observed on June 17, 2011 before corrections were implemented. These observed errors are compared to errors predicted by the error model, demonstrating a good fit.

4.4. Tracking Error Observations after Corrections

The tracking error correction method of Section 3.2 was used in attempt to focus a beam from the heliostat "12E13" onto a target located on North face of the tower, along the tower centerline, and 25.0m above the ground on July 15, 2011. The test day featured wind speeds from 5-20 mph and scattered clouds. Eq. 12 was solved numerically, using the error parameter vector calculated in Section 4.3, to calculate adjusted heliostat pointing angles for every time step from 12:53 p.m. – 4:30 p.m. The heliostat pointing errors were calculated, using the image acquisition setup described in Section 4.2, every ~3-4 minutes.

The tracking errors observed with the correction algorithm in place are compared to the uncorrected errors predicted by Eq. 9 in Fig. 8, demonstrating a significant improvement. The error model predicted that uncorrected tracking errors would range from 4.0 – 8.3 mrad in azimuth, and 4.7 – 7.2 mrad in elevation. With tracking error correction in place, the rms tracking errors were reduced to 0.4 mrad in azimuth and 0.1 mrad in elevation. The high-frequency fluctuations of the observed errors indicate that the errors were primarily due to heliostat shaking in the presence of the 5-20 mph winds. The azimuthal fluctuations are more prominent than the elevation fluctuations, probably because the elevation gears are gravity-loaded, whereas the azimuth gears provide little resistance to the wind within the drive backlash. The rms errors after correction could be expected to be further improved on a day with calmer winds.

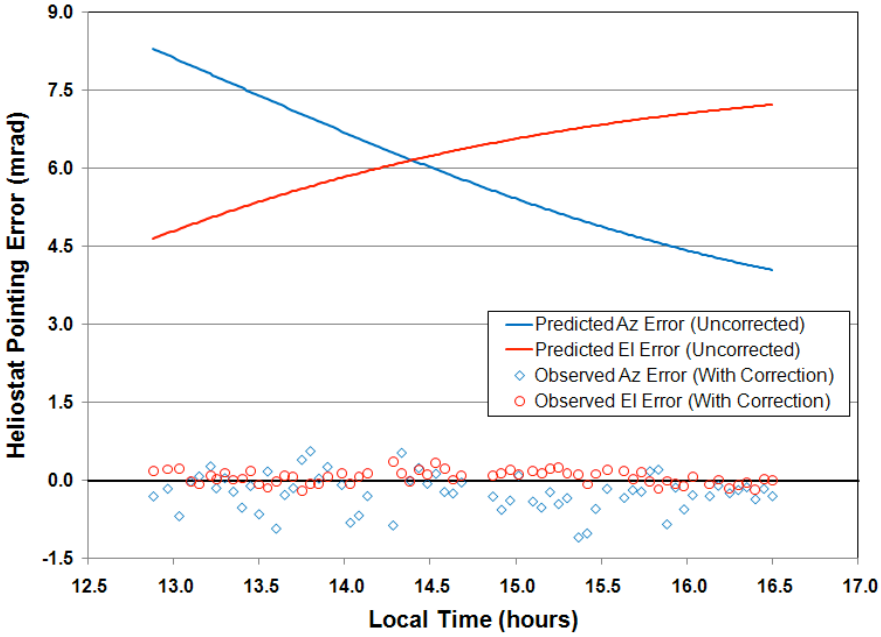

Fig. 8. Plot of heliostat pointing errors observed on July 15, 2011 after error corrections were implemented. These observed errors are compared to errors predicted by the error model (if left uncorrected), demonstrating a significant improvement.

4.4. Analysis of Error Contributions

The error model described by Eq. 9 can be used to estimate the individual contributions of each physical error source to the overall heliostat pointing error (Table 2). The estimated contributions of the individual error sources to the expected azimuthal and elevation pointing errors (if left uncorrected) during the period of observation on July 15, 2011 are plotted in Fig. 10. The most prominent error sources contributing to the azimuthal error were pedestal tilt, boresight error, and drive-axis non-orthogonality. In this case, the drive-axis non-orthogonality tended to reduce the impact of the azimuthal errors introduced by the pedestal tilt and boresight error. The most prominent error source contributing to the elevation error was pedestal tilt.

Table 2. Contributions of individual error sources to the heliostat pointing errors in azimuth and elevation.

Error Source	Contribution to Azimuthal Pointing Error	Contribution to Elevation Pointing Error
Pedestal Tilt	$\varepsilon_1 \sin\theta \tan\alpha + \varepsilon_2 \cos\theta \tan\alpha$	$\varepsilon_1 \cos\theta - \varepsilon_2 \sin\theta$
Reference Bias	ε_3	ε_4
Linear Errors	$\varepsilon_5\theta$	$\varepsilon_6\alpha$
Drive-Axis Non-Orthogonality	$\varepsilon_7 \tan\alpha$	0
Boresight Error	$\dfrac{\varepsilon_8}{\cos\alpha}$	0

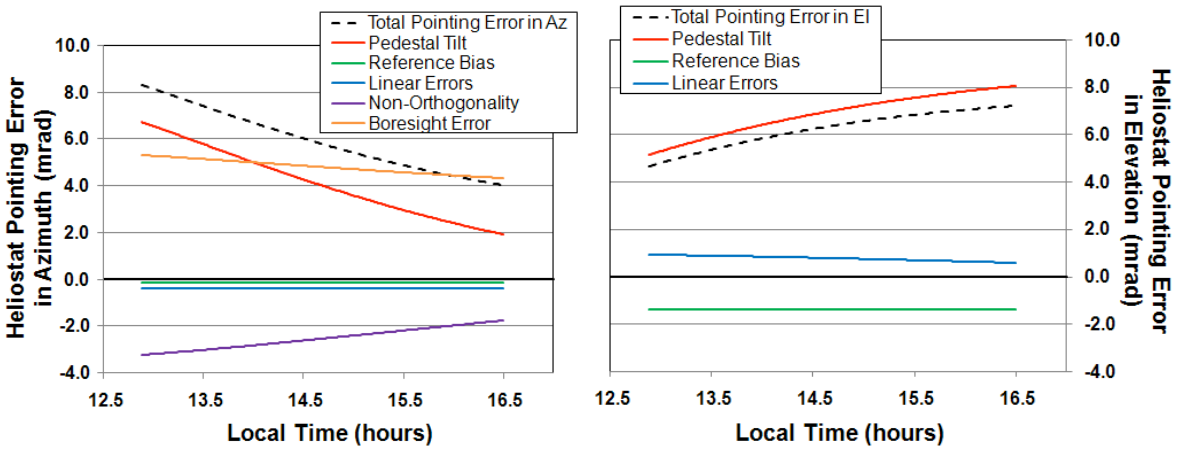

Fig. 10. Plot of estimated contributions of individual error sources predicted by the error model (if left uncorrected) during the period of observation on July 15, 2011.

5. Summary

Accurate heliostat tracking is critical for the overall performance and efficiency of a central receiver concentrating solar power plant. Subtle errors in the fabrication and installation of heliostats can cause tracking errors that change throughout the day and year due to their non-linear dependence on the intended pointing vectors. The impact of these errors is exacerbated when a heliostat is located far from its target and can cause the reflected beam to miss the target, resulting in inefficiencies in the power plant's performance. It is typically not feasible to repair these fabrication and installation errors after heliostats are installed. Implementing a fixed pointing offset is usually ineffective due to the dependence of the errors on the time of day, day of the year, and target location. This paper described an automated open-loop eight-dimensional tracking error characterization and correction method that is suitable for large heliostat fields, as it does not require any physical modification to the heliostats and may allow for a more rapid data collection relative to methods that use on-axis tracking. Tests were performed on a heliostat at the National Solar Thermal Test

Facility at Sandia National Laboratories in Albuquerque, NM using this method, and analyses were performed to evaluate the relative contributions of the various error sources. Uncorrected heliostat pointing errors ranging from 4.0 – 8.3 mrad in azimuth and 4.7 – 7.2 mrad in elevation were reduced to rms errors of 0.4 mrad in azimuth and 0.1 mrad in elevation, in the presence of wind speeds as high as 20 mph. Ongoing efforts continue the measurement of tracking error improvements throughout the year.

Acknowledgments

The authors thank Gregory J. Kolb (Sandia National Laboratories) for motivating this work, tilting the heliostat, and contributing to data collection. The authors also thank Edward J. Smith and Michael A. Usher (Sandia National Laboratories) for operating the heliostat during testing.

Sandia National Laboratories is a multi-program laboratory managed and operated by Sandia Corporation, a wholly owned subsidiary of Lockheed Martin Corporation, for the U.S. Department of Energy's National Nuclear Security Administration under contract DE-AC04-94AL85000.

References

[1] Baheti, R.S. and P.F. Scott, 1980, "Design of Self-Calibrating Controllers for Heliostats in a Solar Power Plant," IEEE Trans. Autom. Control, Vol. AC-25, No. 6, 1091-1097.

[3] Edwards, B., 1981, "A Computational Alignment Method for Paraboloidal Collectors," Sol. Energy, Vol. 26, Issue 2, pp. 121-125.

[5] Mavis, C.L., 1988, "10 MWe Solar Thermal Central Receiver Pilot Plant Heliostat and Beam Characterization System Evaluation November 1981 – December 1986," SAND87-8003, Sandia National Laboratories, Livermore, CA. (http://infoserve.sandia.gov/sand_doc/1987/878003.pdf)

[6] Maish, A.B., 1991, "The Solartrak Solar Array Tracking Controller," SAND90-1471, Sandia National Laboratories, Albuquerque, NM. (http://infoserve.sandia.gov/sand_doc/1990/901471.pdf)

[8] Stone, K.W. and S.A. Jones, 1999, "Analysis of Solar Two Heliostat Tracking Error Sources," SAND99-0239C, in Proceedings of the 1999 ASME International Solar Energy Conference, Maui, HI, April 11-14, 1999, 8 pp.

[10] Jones, S.A. and K.W. Stone, 1999, "Analysis of Strategies to Improve Heliostat Tracking at Solar Two," SAND99-0092C, in Proceedings of the 1999 ASME International Solar Energy Conference, Maui, HI, April 11-14, 1999, 8 pp.

[12] Chen, Y.T., B.H. Lim, and C.S. Lim, 2006, "General Sun Tracking Formula for Heliostats with Arbitrarily Oriented Axes," J. Sol. Energy Eng., Vol. 128, Issue 2, pp. 245-250.

[14] Chong, K.K., C.W. Wong, F.L. Siaw, T.K. Yew, S.S. Ng, M.S. Liang, Y.S. Lim, and S.L. Lau, 2009, "Integration of an On-Axis General Sun-Tracking Formula in the Algorithm of an Open-Loop Sun-Tracking System," Sensors, Vol. 9, Issue 10, pp. 7849-7865.

[16] Guo, M., Z. Wang, W. Liang, X. Zhang, C. Zang, Z. Lu, and X. Wei, 2010, "Tracking Formulas and Strategies for a Receiver Oriented Dual-Axis Tracking Toroidal Heliostat," Sol. Energy, Vol. 84, Issue 6 pp. 939-947.

[17] Draper, N.R. and H. Smith, 1966, *Applied Regression Analysis*. New York: Wiley.